Dispersive Wave Analysis – Method and Applications

Rama Rao V. N. and M. Nafi Toksöz
Earth Resources Laboratory
Department of Earth Atmospheric and Planetary Sciences
Massachusetts Institute of Technology
Cambridge, MA 02139

Abstract

A technique for estimating the dispersion characteristics of propagating waves as measured by an array is detailed. The technique consists of bandpass filtering the data through a filterbank and then processing the filtered waveforms non-dispersively. The results can show the dispersion of the entire time series or be parsed in time to analyze the dispersion characteristics of any section of the time series. Processing LWD field data shows that this method can extract dispersion characteristics over a broadband of frequencies and with low amplitude signals. Both the field data and laboratory scale data show that multiple modes present over the same frequency band can be identified.

1 Background

Logging while drilling (LWD) measurements are increasingly finding use in critical and expensive drilling scenarios. With a large tool in the borehole (relative to wireline measurements), LWD data is most often characterized by modal response of the formation and the tool in the borehole, in addition to refracted arrivals. This is more so in slow formations when modal arrivals are the only option for extracting formation shear properties. In presence of complications like tool offcentering, non-circular boreholes and anisotropy the dispersion effects can be more pronounced. Since modal responses are often recorded as weak to strongly dispersed wavetrains, inverting for formation shear involves processing the data to obtain the dispersion characteristics of the data and then interpreting/inverting the formation speeds from it. We describe a technique to do the former along with illustrations of its use with field and laboratory scale data.

2 Introduction

A common technique for processing acoustic array data is the slowness time coherence (STC) method (Kimball and Marzetta 1984, Neidell and Taner, 1971). This method is very robust and can work with multiple wavetypes and with weak arrivals, giving reliable results if the recorded waves are non-dispersive i.e., phase and group speeds are independent of frequency. But in reality, many of the arrivals that are recorded, like the flexural, pseudo-rayleigh and screw modes, are dispersive. In such cases, non-dispersive processing methods like STC produce biased estimates of formation properties.

Many of the common dispersive processing approaches include prony's method, maximum entropy (ARMA) methods (Kay and Marple, 1981), and predictive array processing (Lang et al, 1987). They typically involve fitting a chosen number of model functions to the data, which requires a choice for the number of modes expected in the data. This choice affects the quality of results as choosing too many or too few leads to spurious results. MLM–based methods tend to ignore weak arrivals and are computationally expensive (Hsu and Baggeroer, 1986). Non-parametric methods are data adaptive in that they typically do not require the above choice. Methods include phase minimization or coherency maximization techniques (Tang et al, 1995), like the homomorphic processing approach (Ellefsen et al., 1993). The latter can resolve only one mode at a given frequency. Conceptually, these methods are a frequency domain analog of the STC.

The processing method given here produces frequency dispersion characteristics of data while allowing for the possibility of parsing the arrivals in time, so that dispersion characteristics of any wave packet propagating across the array can be isolated.

3 The Approach

The principle is to bandpass the data through multiple frequency bands such that the output of each band can be processed non-dispersively. If the waves in the measurements were non-dispersive, no filtering would be necessary and non-dispersive velocity analysis methods like STC can be applied to estimate their phase speed. However, both dispersive and non-dispersive waves are commonly present and their characteristics vary depending on many parameters, including the logging tool type (wireline or LWD), source and receiver type (monopole, dipole, quadrupole) and borehole and formation properties.

The choice of number of filter bands must be made based on the desired frequency resolution, computational speed considerations or some combination of both. In this paper we illustrate the concept with uniformly spaced center frequencies. We choose constant relative bandwidth gaussian filters for their optimal space-time resolving capability (Dziewonski et al, 1969). This implies that the ratio of the bandwidth to the center frequencies of the filters is a constant.

The flowchart of processing is in Figure 1. Let the time series measured at these locations be $w_i(t)$. In pre-processing, the time series $w_i(t)$ are processed to mitigate noise and enhance data quality. The filter bank properties such as the center frequencies of the filters, filter widths and filter shape are specified. The steps of data filtering with a filterbank, downsampling, and interpolating may also be implemented by wavelet based filterbank methods.

Filtering the data with the filter bank is followed by decimation. Data in the low frequency bands is sampled much higher than is necessary and is decimated. Data in the higher frequency bands can (optionally) be demodulated and shifted to low frequencies and also be decimated. The decimation allows velocity analysis to be performed over much fewer time samples and speeds it up.

Velocity analysis is then performed. Any type of velocity analysis, appropriate for non-dispersive or weakly dispersive data, like semblance analysis (STC) may be performed on the decimated output of the each of the filter banks. This step can be generalized for any expected moveout (linear, hyperbolic,…) depending on the data, by appropriately modifying the velocity analysis calculation. The velocity analysis results, with different time sampling in different frequency bands, may be interpolated to bring all results to a common sampling rate.

The results are now a data cube of phase speed, frequency and arrival time. The results can be interpreted/used at different levels. Plotting the coherence/semblance of phase speed versus frequency for successive time instances as a movie, exemplifies the dispersive character of the observed waves as time evolves. Given a time window (and, say, frequency band and speed/slowness band) of interest, the corresponding sub volume of data can be collapsed along the time axis to extract the dispersion characteristics. At each phase speed /frequency combination, the semblance values at different times form an array, and ‘collapsing’ along the time axis consists of obtaining a single representative semblance value from this array of values. The maximum operator may be used. This provides a synthesis of the dispersion characteristics of all wave types within the time window of interest. Finally this operation can be also done over the entire time record to get the dispersion characteristics of all observed waves.

Once the dispersion features in phase speed and frequency have been derived, phase dispersion curves can be extracted by tracking the peak semblance values. Group dispersion curves can be calculated from the phase dispersion curves based on the standard relations between them.

4 Field Data

The filtered frequency semblance approach is illustrated by an analysis of field data. The purpose is to exemplify possible types of analysis that may be done. The data is from a dipole LWD measurement with a source operating in the 5-7 [kHz] range.

4.1 Formation Compression speed estimation
Time series data from three different depths are shown in Figure 2. Of the two receiver arrays, the front array timeseries is displayed. Note the high noise level in Case 140. Figure 3 shows the results of performing the filtered frequency semblance on the data. Hot colors identify significant responses.

The two main aspects of Figure 3 are the feature at 2500-3000 [m/s] and at 12-20 [kHz] and the peaks around 1000 [m/s] between 3-15 [kHz]. The former can be identified as the compressional arrival while the latter are modal arrivals which will be identified in a future section. Figure 4 shows the spectral amplitudes of all receivers. The coherence peak corresponding to the compressional response arises from very low amplitude spectral components. In fact, the spectral amplitudes above 12 [kHz] are about 2 orders of magnitude or 40 [dB] below the peak spectral amplitude. Figure 5 shows the original timeseries data filtered between 12-20 [kHz]. The dominant moveout at early times matches the compressional speed observed in Figure 3. Thus despite low amplitudes the compressional arrival was clearly identified in Figure 3 because of its coherent presence across the array. This illustrates that usable information when present at higher frequencies in field data and can be extracted despite poor signal-to-noise, with this approach.

4.2 Case 060: Front and back array data asymmetry
The results of independently processing the front and back array at depth x060 with filtered frequency semblance are shown in Figure 6. Dipole mode curves are overlaid and appear to match the observed features reasonably. The implied formation shear speed is shown (dashed yellow line).

It is well established that the Stoneley mode dispersion is very similar to that of the formation flexural mode at except at low frequencies, e.g., 4 [kHz] and higher in this case. To ascertain whether the observed features are dipole or monopole in character, we first identify the frequency, speed and time ranges of the data that contribute to the observed feature. The frequency and speed ranges are obtained by inspection of Figure 6 as 2.5 [kHz] and 900-1000 [m/s]. The time range can be ascertained by parsing the 3D output of the filtered frequency semblance along the time axis to identify the time interval when the feature is present. Based on this approach, the time range is 1-2 [ms]. Figure 7 shows the data filtered in the above frequency band with the time and speed ranges highlighted in gray. It can be seen that within this region the front and back array are mainly out of phase, i.e., they are composed of one or more anti-symmetric modes like dipole, hexapole, decapole etc. However, given that the dispersion character in Figure 6 matches the dipole mode, we can conclude that the features are dominantly dipole responses.

The observed dispersion is different between the front and back array. The coherence peak in the front array appears to be faster compared to that on the back array. Tool off-centering or non-circular boreholes will cause the dipole mode to split into two dipole modes (Zheng et al, 2004). One of the modes propagates faster while the other propagates slower, relative to the dipole mode of the centered case. Given the unequal time series amplitudes and this dispersion characteristic, we can conclude that tool and/or the borehole asymmetry is present.

4.3 Case 140: Quadrupole response
The frequency semblance results for the front and back array at depth x140 are shown in Figure 8. Again the front and back array appear to measure different modal responses. The back array has features that align with dipole, quadrupole and hexapole dispersions while only the dipole dispersion is relevant in the front array.

A data cube in phase speed, frequency and time that gives rise to the feature coinciding with quadrupole dispersion is isolated in Figure 9. While the data at this depth is noisy, with moveouts corresponding to waves propagating towards the source, the front and back array are approximately in phase within the highlighted region, relative to outside of the region. This indicates that a quadrupole response is in fact being measured.

Figure 10 displays the results of similarly filtering the data for identifying the remaining features in Figure 8. The out of phase responses indicate that dipole and hexapole responses are being measured.

4.4 Case 000: Decapole response ?

Time series of the front and back array are displayed in Figure 11 with the filtered frequency semblance result in Figure 12. In the frequency semblance, the front and back features align with dipole mode dispersion, while in the back array there is additionally a weak feature that matches the decapole dispersion. The differences in the front and back dispersions suggests tool off-centering and/or non-circular borehole. Given the weakness of the feature matching the decapole response, further analysis is required to confirm its presence.

5 Laboratory Data

Data was acquired from a scaled LWD tool operating in an orthorhombic formation. Boreholes were drilled at multiple angles relative to the anisotropy and data from a scaled LWD tool was collected to simulate measurements in highly deviated holes.

5.1 Experiment setup

A scaled LWD tool (about 1:17 scale) was used in the experiment (Zhu et al 2003). It consists of a multipole source capable of firing as a monopole, dipole (two perpendicular orientations) and a quadrupole (two perpendicular orientations). The receiver array consists of six dipole receivers.

The formation is a block of Phenolite (Figure 13a). The blocks were machined such that the square cross-section of the XY plane was converted to a polygon. This corresponded to two parallel block faces at angles 0, 15, 30, 45, 60, 75, 90, 105, 120, 135, 150 and 165 degrees. Time of flight measurements were made with transducers across perpendicular faces to obtain the various body wave speeds at these azimuths. Then boreholes were drilled perpendicular to these faces so that measurements with the scaled LWD tool in borehole could be made along seven azimuths (0, 15, 30, 45, 60, 75 and 90 degrees).

Two types of measurements were made at each azimuth – dipole and cross dipole. They are as illustrated in Figure 13 b. The X direction corresponds to the fast direction while the Y corresponds to the slow direction. The dipole operation consists of the source and receiver dipoles aligned along the formation fast direction (X). The Cross dipole operation consists of the source dipole along the slow direction (Y) with the receiver dipole is aligned with the fast direction (X). The multipole source allowed the collection of the dipole and cross dipole data without any physical disturbance in the setup as it only involved electronically switching the source transducers appropriately.

5.2 Data Analysis

Data was recorded for the seven azimuths and processed with the filtered frequency semblance method. The results for the dipole case are shown in Figure 14. The seven panels show the observed dispersions along with best fitting dipole and hexapole curves overlaid. The implied formation shear speeds are shown as dashed yellow lines. It can be seen that a hexapole response is present in many cases as evidenced by the match between the processing results and the hexapole dispersions. Formation compression peaks are also present in the data, though not shown. The formation speeds thus estimated from the dispersion analysis is summarized in Figure 15. In all three plots the black lines indicate the time of flight measurements while the colored markers show the speeds estimated from LWD measurements.

The compression speed estimates have a trend comparable to the time of flight measurements with mean absolute deviations of 2.9 %. Discrepancies are from phenolite machining errors which give rise to small variations in propagation path (~0.5%), measuring group speed (~0.5%) and measurement errors.

The formation shear speed can be estimated from the dipole modes and hexapole modes. With the source and receiver aligned along the fast direction, the fast dipole mode is measured at all azimuths. The slow dipole mode is technically along the null of the receivers and should not be observed. But given finite sized transducers and receiver arrays being not exactly aligned with the fast direction, the slow dipole mode

is also measured, at 0, 15, 60, 75 and 90 degrees. In this orientation, the hexapole modes asymptoting to the slow formation shear speed are only observed.

The same measurements were repeated for the Cross dipole configuration (Figure 13). The frequency semblance results of analyzing data at all azimuths are shown in Figure 16. Again fast and slow dipole modes are identified, whenever present. The results are summarized in Figure 17. With the source nominally aligned along the slow direction, slow dipole modes are dominantly excited along with weak fast dipole modes. With the receivers nominally along the fast direction, both dipole responses are recorded. However, the slow dipole mode and consequently the slow shear speed is the consistent measurement, present in all but one azimuth.

Overall the deviations in the shear measurements are between 2.8 - 4.7 %. In addition to the errors mentioned for the compressional measurements, the shear speed estimates have an additional source of error. While compression speeds were estimated directly from refracted arrivals, shear speeds were estimated by fitting the observed dipole and hexapole dispersion characteristics in the frequency semblance with theoretical dispersion curves. The theoretical dispersion curves were from equivalent isotropic formation models. These isotropic dispersion curves match the anisotropic dispersions reasonably, but not exactly. A comparison between anisotropic and an equivalent isotropic dispersion curves for a TIH case is illustrated in Sinha et al 2000. Hence the use of approximate dispersion curves biases the shear speed estimates and contributes to the deviations.

5.3 Discussion

LWD dipole data collected in the orthorhombic formation measured the fast and slow formation shear speeds. In general, one or both formation shear speeds may be measured depending on the alignment of the source and receiver arrays relative to the principal directions.

Dipole modes tend to be sensitive to formation shear speeds that are parallel to their direction i.e., a dipole mode polarized along a principal direction (say X) is sensitive to the formation shear speed along the X direction. Hexapole mode appears to differ from the dipole in this aspect. With the source and receivers aligned along the fast direction (dipole operation), the observed hexapole modes were asymptotic to the *slow* formation shear speed. In the Cross dipole operation, this would imply that the hexapole modes will asymptote to the fast formation shear. However no hexapole response was observed in this case. The schematics of a dipole and hexapole distribution are shown in Figure 18, indicating the null directions for each of them. Figure 19 summarizes the dipole and hexapole distributions relative to the formation anisotropy and source/receiver orientations. This suggests that in the Cross dipole operation, the receivers are in the nulls of the slow dipole mode and the fast hexapole mode. We observe the former but not the latter. Our current hypothesis is that, for the transducer sizes being used, the pressure cancellation at the receivers along the hexapole null directions is more effective, than that for the dipole case.

The logical next steps in this study are theoretical confirmation of the hexapole mode sensitivity to formation shear perpendicular to its orientation and the relative strengths of dipole and hexapole responses near their null directions.

6 Conclusion

A technique for extracting dispersion characteristics of signals in array data is presented**.** The key steps involve filtering the data into multiple frequency bands and then performing STC or similar processing on the filtered data. It is applied to field LWD data and laboratory scale LWD measurements. In the field data, with a source firing in the 5-7 [kHz] range, refracted arrivals in the 12-20 [kHz] range and modal arrivals up to 15 [kHz] were meaningfully interpreted. With the laboratory scale data, modes could be identified up to 250 [kHz] which corresponds to about 15 [kHz] in the full scale situation. Thus this approach has the potential for broadband processing and interpretation of array data. Dispersion features from low amplitude signals can be extracted due to the amplitude normalization implicit in the STC calculation. Further, this processing method can identify as many modes as there are in the data without prior guesses at

their number. With field and laboratory data in both isotropic and anisotropic situations, multiple modal arrivals at a single frequency could be identified and interpreted.

7 Acknowledgements

We wish to acknowledge Dr. Zhenya Zhu for collecting the data in the phenolite borehole. We wish to acknowledge Dr. Brian Hornby and BP for providing the field data for analysis. This work was supported by the Earth Resources Laboratory Borehole Acoustics and Logging Consortium and the Founding Members of the Earth Resources Laboratory with additional support from Halliburton Energy Services.

References

Dziewonski, A., Block, S., and Landisman, M., 1969, A technique for the analysis of transient seismic signals, Bull. Seis. Soc. Am., 59, 427-444.

Ekstrom, M. P., 1996, Dispersion estimation from borehole acoustic arrays using a modified matrix pencil algorithm, Presented at the 29 Asilomar Conference on Signals, Systems and Computers.

Kay, S. M., and Marple, S. L. Jr.,1981, Spectrum Analysis – a modern perspective, Proc. Inst. Electr. Electron. Engg., 69, 1380-1419.

Kimball, C. V., and Marzetta, T. L., 1984, Semblance processing of borehole acoustic array data, Geophysics, 49, 274-281.

Hsu, K., and Baggeroer, A. B., Application of maximum-likelihood method (MLM) for sonic velocity logging, Geophysics, 51(3), 780-787.

Lang, S. W., Kurkjian, A. L., McClellan, J. H., Morris, C. F. and Parks, T. W., 1987, Estimating slowness dispersion from arrays of sonic logging waveforms, Geophysics, 52, 530-544

Neidel, N. S., and Taner, M. T., 1971, Semblance and other coherency measures for multi-channel data, Geophysics, 36, 482-497.

Sinha, B. K. Kane, M. R., and Frignet, B., 2000, Dipole dispersion crossover and sonic logs in a limestone reservoir, Geophysics, 65(2), 390-407.

Tang, X. M., 1997, Predictive processing of array acoustic waveform data, Geophysics, 62(6), 1710-1714.

Zheng, Y, Huang, X, Toksoz, M. N., 2004, A finite element analysis of the effects of tool eccentricity on wave dispersion properties in borehole acoustic logging while drilling, ERL Industry Consortium Report.

Zhu, Z., Rao, R., Burns, D. R., Toksoz, M. N., 2004, Experimental studies of multipole logging with scaled borehole models, ERL Industry Consortium Report.

Figure 1

Flow chart of processing

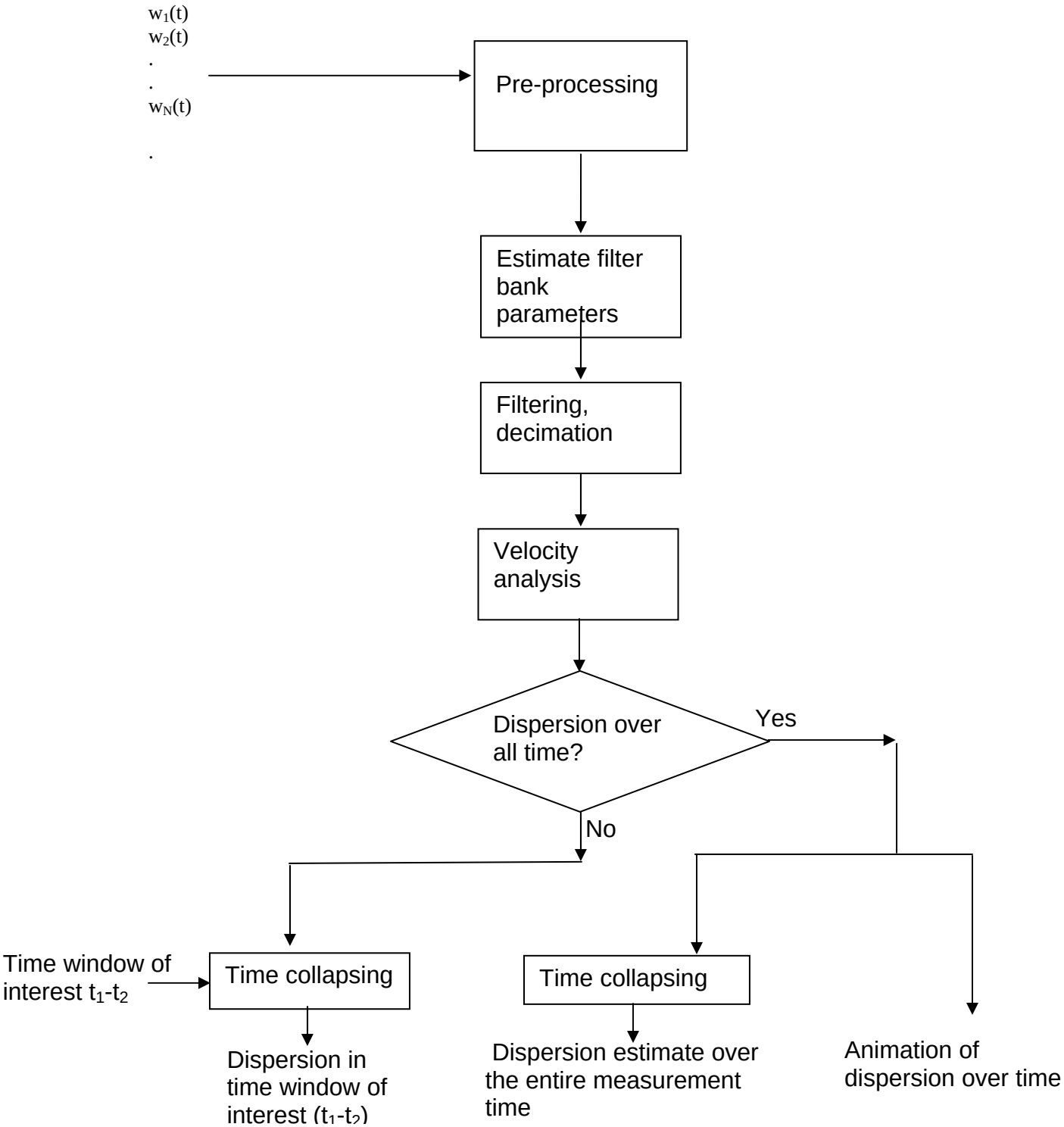

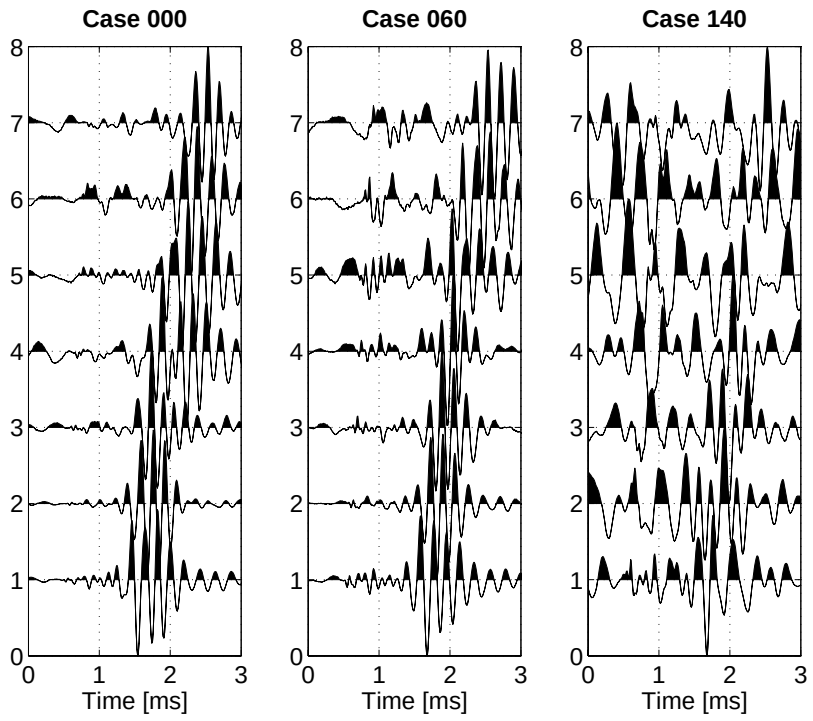

Figure 2: LWD data at three depths, for a source frequency in the 5-7 [kHz] range. Front array timeseries is shown

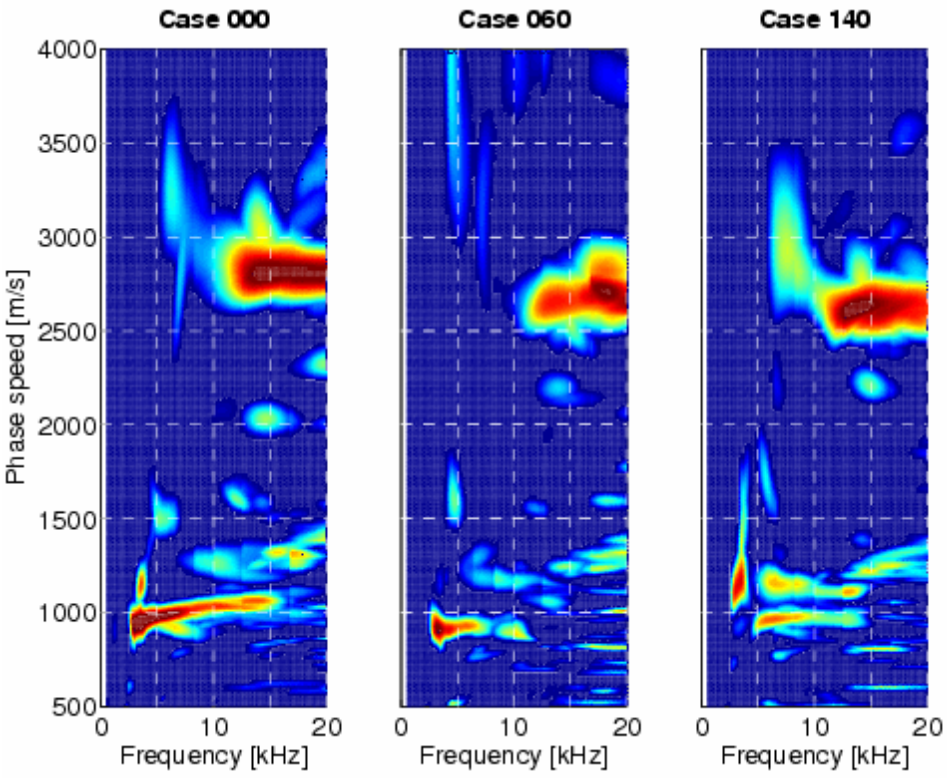

Figure 3: Frequency Semblance of the above data. Note the presence of compression response between 2500-3000 m/s at frequencies above 12 [kHz]. The peaks around 1000 [m/s] correspond to flexural modes. Hot colors identify coherent responses

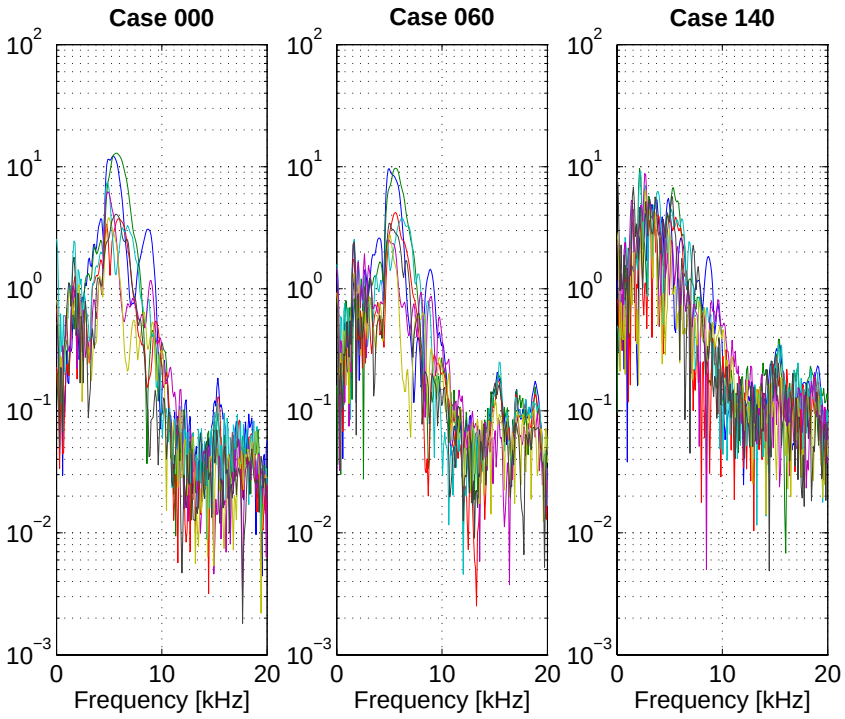

Figure 4: Amplitude spectra of all seven receivers. Note that the compression response observed in 12-20 [kHz] range in Fig 3 is from spectral components that are about 2 orders of magnitude (40 [dB]) below peak amplitude

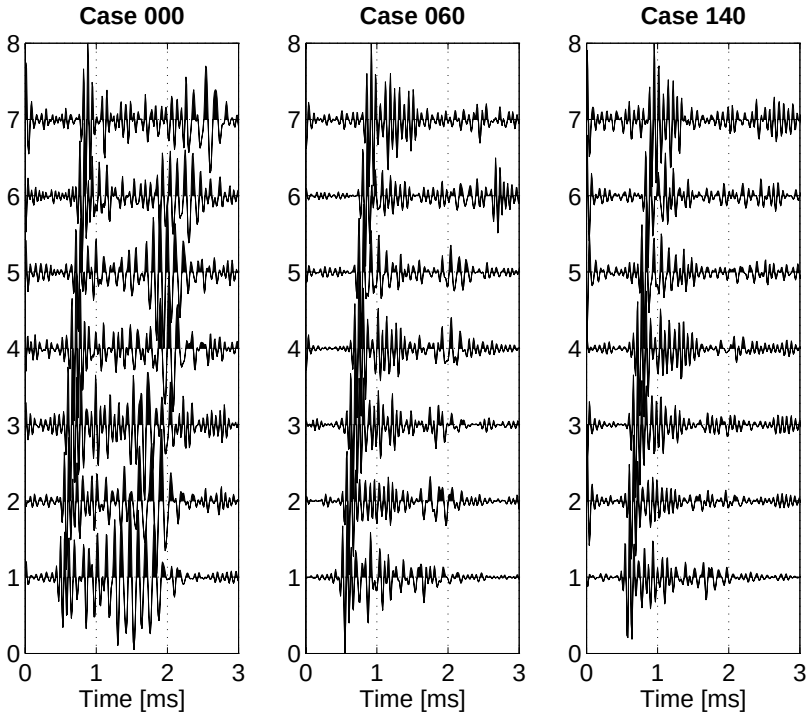

Figure 5: Data filtered between 12 -20 [kHz] clearly showing the compressional moveout at early times illustrating the feasibility of using data even up to 20 [kHz], with source operating in 5-7 [kHz] range

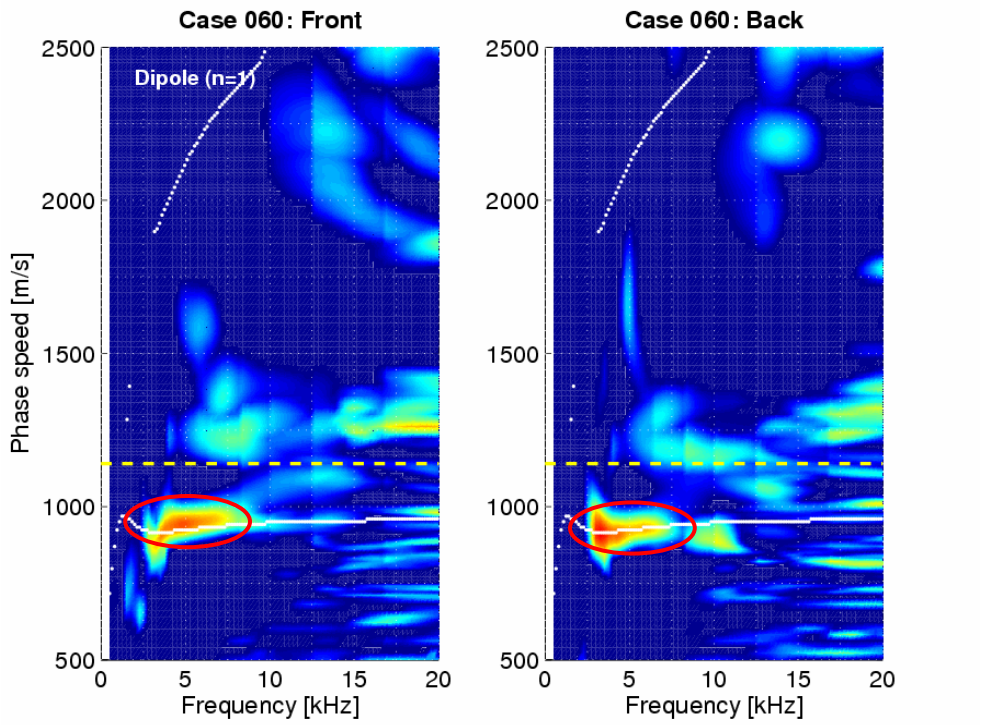

Figure 6 : LWD data, front and back array processed results, along with interpreted dipole modes and formation shear speed (dashed yellow) overlaid. The highlighted feature is due to data between 2.5 – 10 [kHz], and 1- 2[ms].

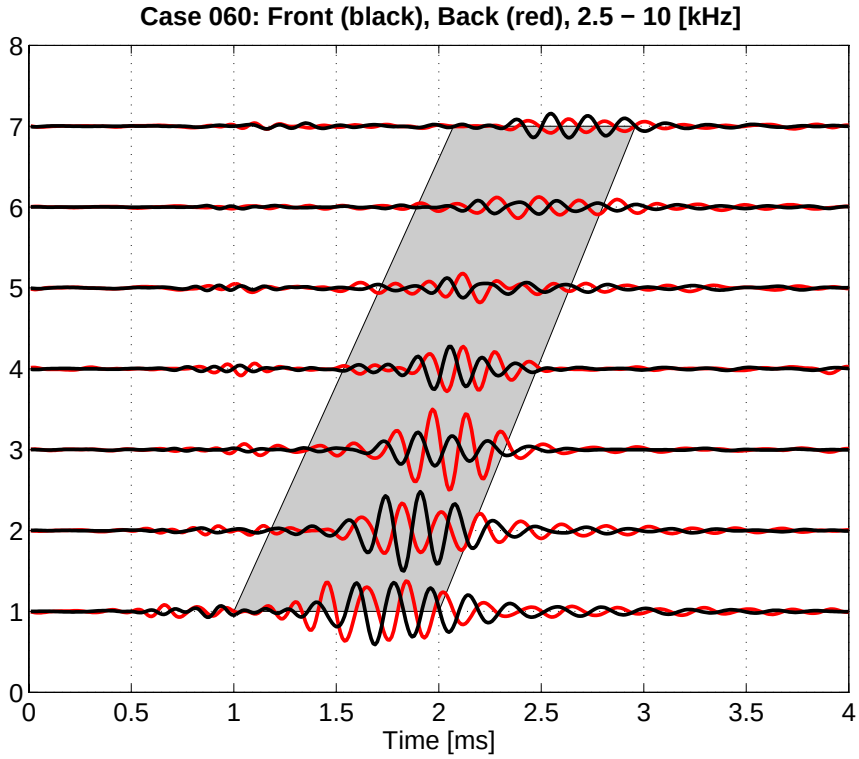

Figure 7 : Data filtered between 2.5 -10 [kHz] shows front and back waveforms are out of phase in the highlighted (gray) time ranges, indicating that the feature in the figure above is dominantly dipole. The difference between the front and back frequency semblance and filtered timeseries amplitudes suggests asymmetry in tool position and/or borehole shape.

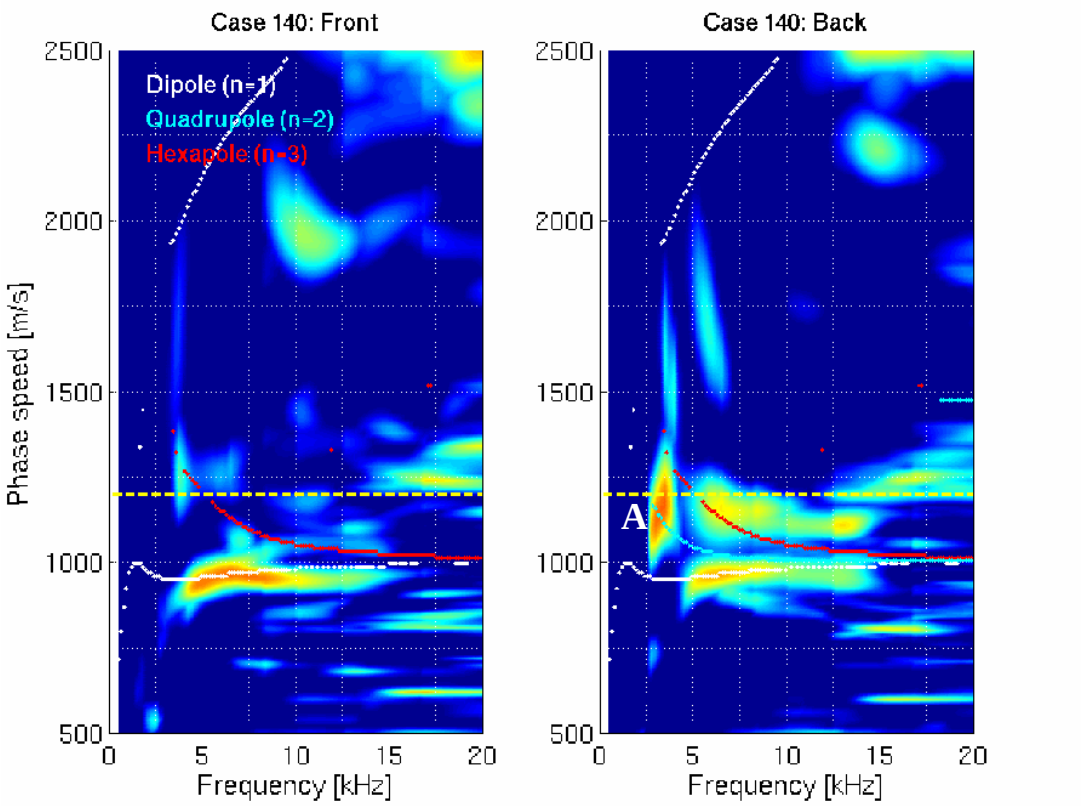

Figure 8 : LWD data, front and Back array processed results. Dipole, quadrupole and hexapole modes and formation shear speed (dashed yellow) overlaid

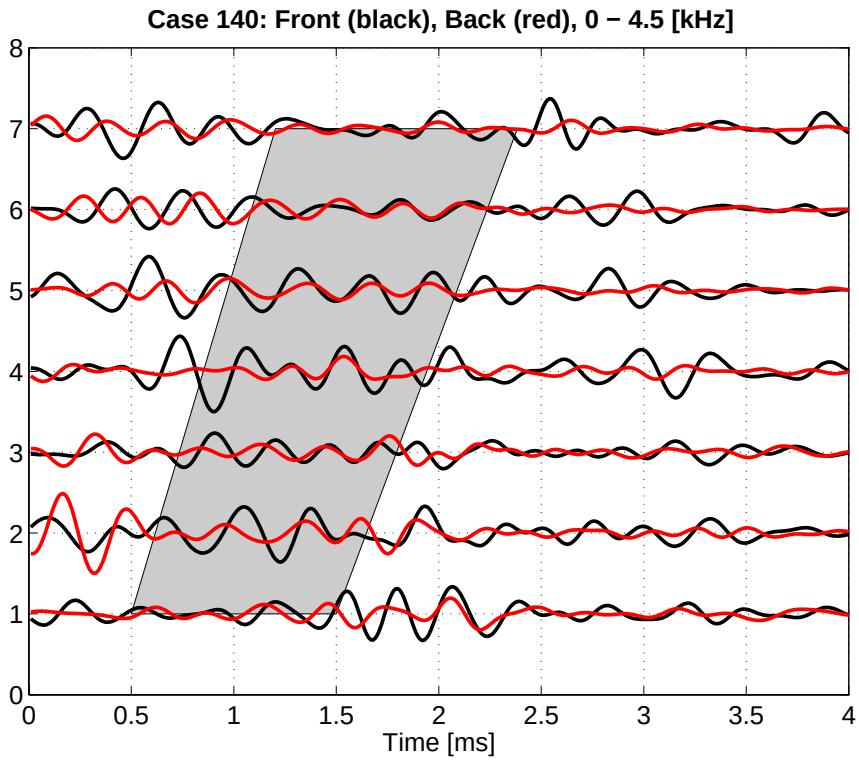

Figure 9 : Data filtered between 0-4.5 [kHz] and highlighted between 0.5-1.5 [ms] generated feature A in previous figure. The front and back waveforms are mostly in phase, indicating that the feature is most likely a quadrupole response

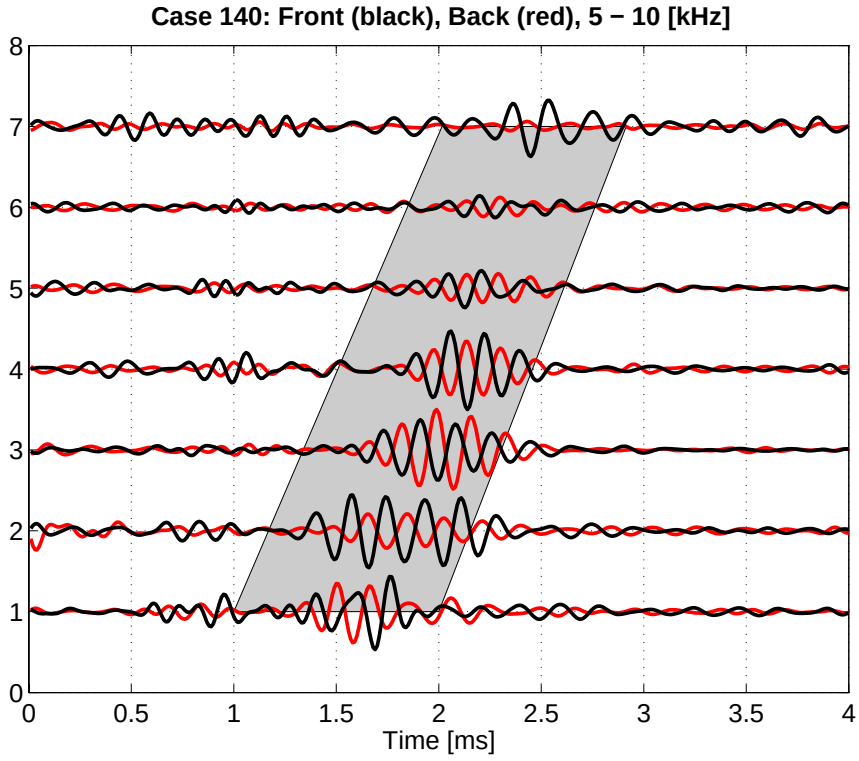

Figure 10: Data filtered between 5-10 [kHz] and highlighted between 1-2 [ms] generated features that align with the dipole and hexapole curves in figure 8. The front and back waveforms are out of phase, confirming their identification

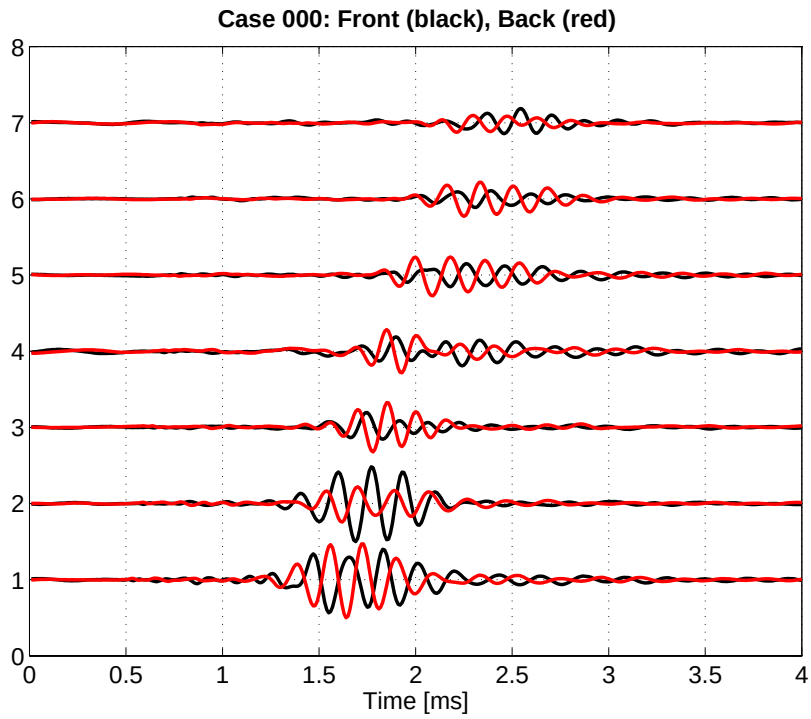

Figure 11 : LWD data, front and back time series, dominantly out of phase

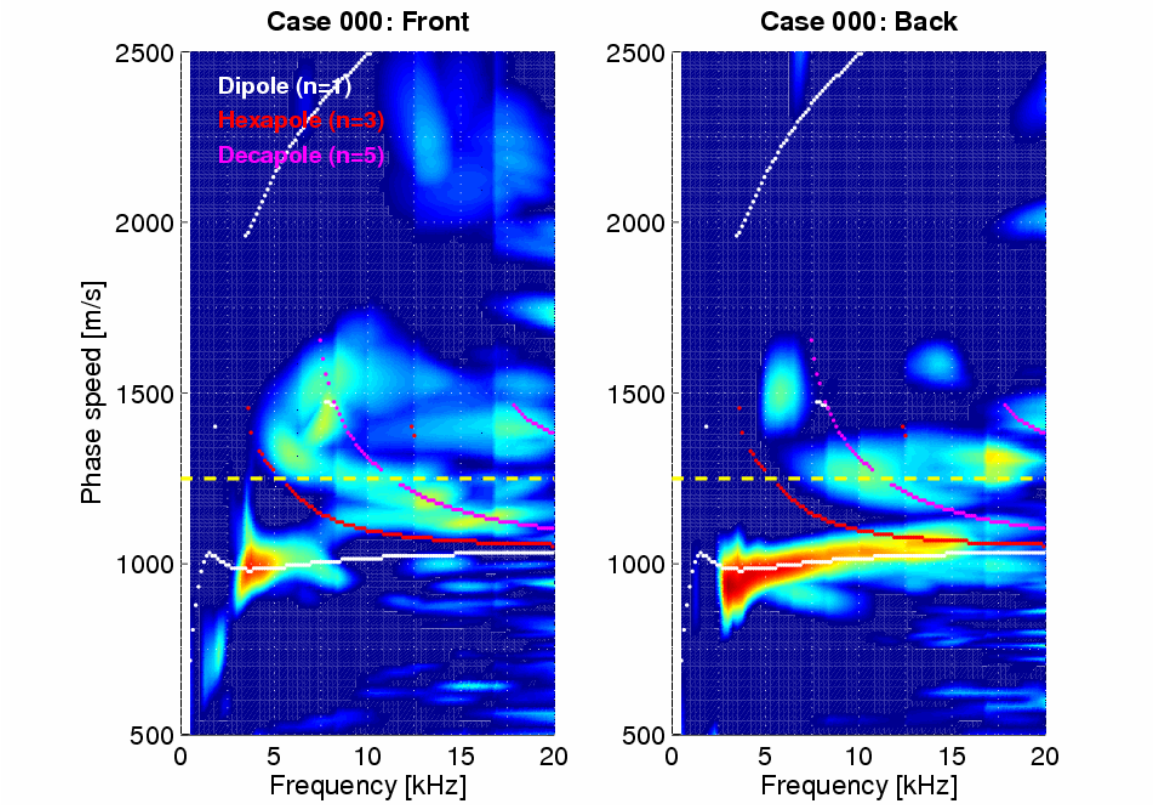

Figure 12 : Filtered frequency semblance result showing presence of dipole and possibly decapole response. The latter needs to be investigated further.

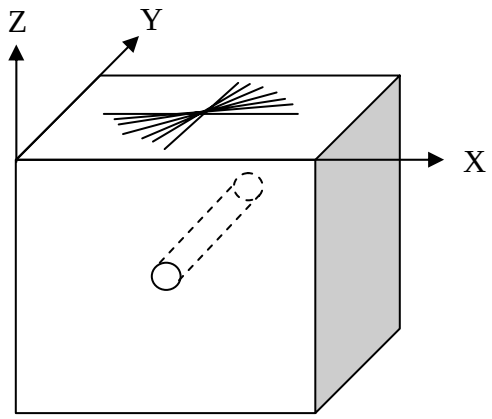

Figure13a : Schematic of phenolite block with a borehole shown parallel to the y-axis. A total of seven non-intersecting boreholes were drilled in multiple blocks with the borehole axis lying in the XY plane and the borehole axis making 0, 15, 30, 45, 60, 75and 90 degrees relative to the X axis (orientations indicated as lines on the top of the block). The symmetry axis of the phenolite blocks are along the z axis.

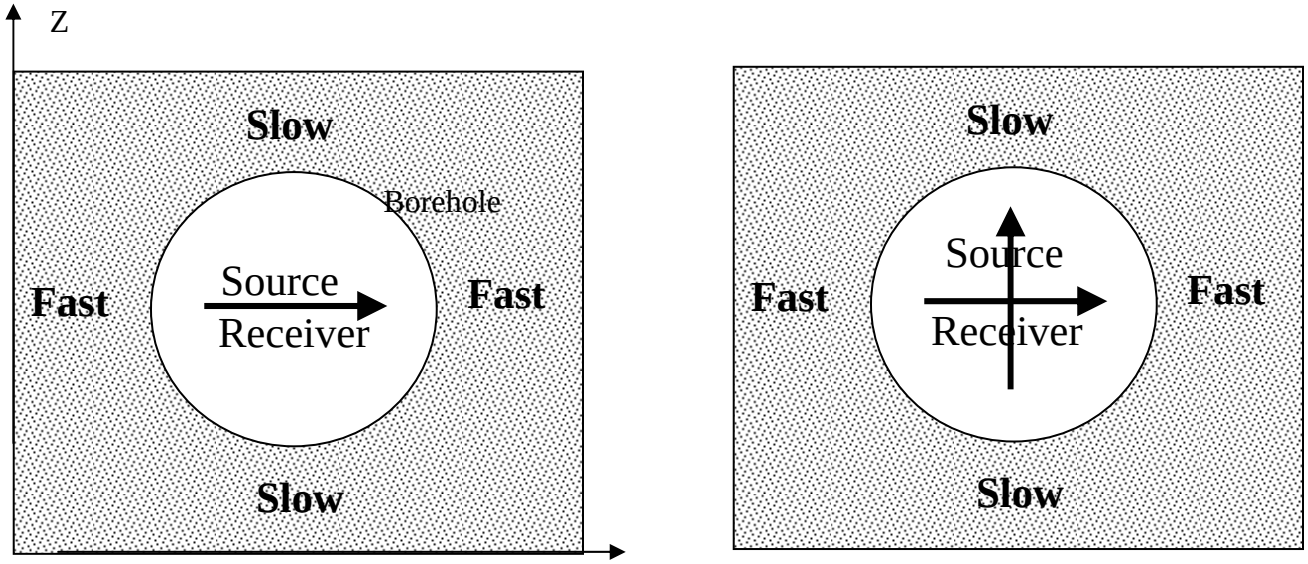

Figure 13 b : Schematic of borehole with alignment of source and receiver dipoles relative to the formation anisotropy in the dipole and cross dipole operation

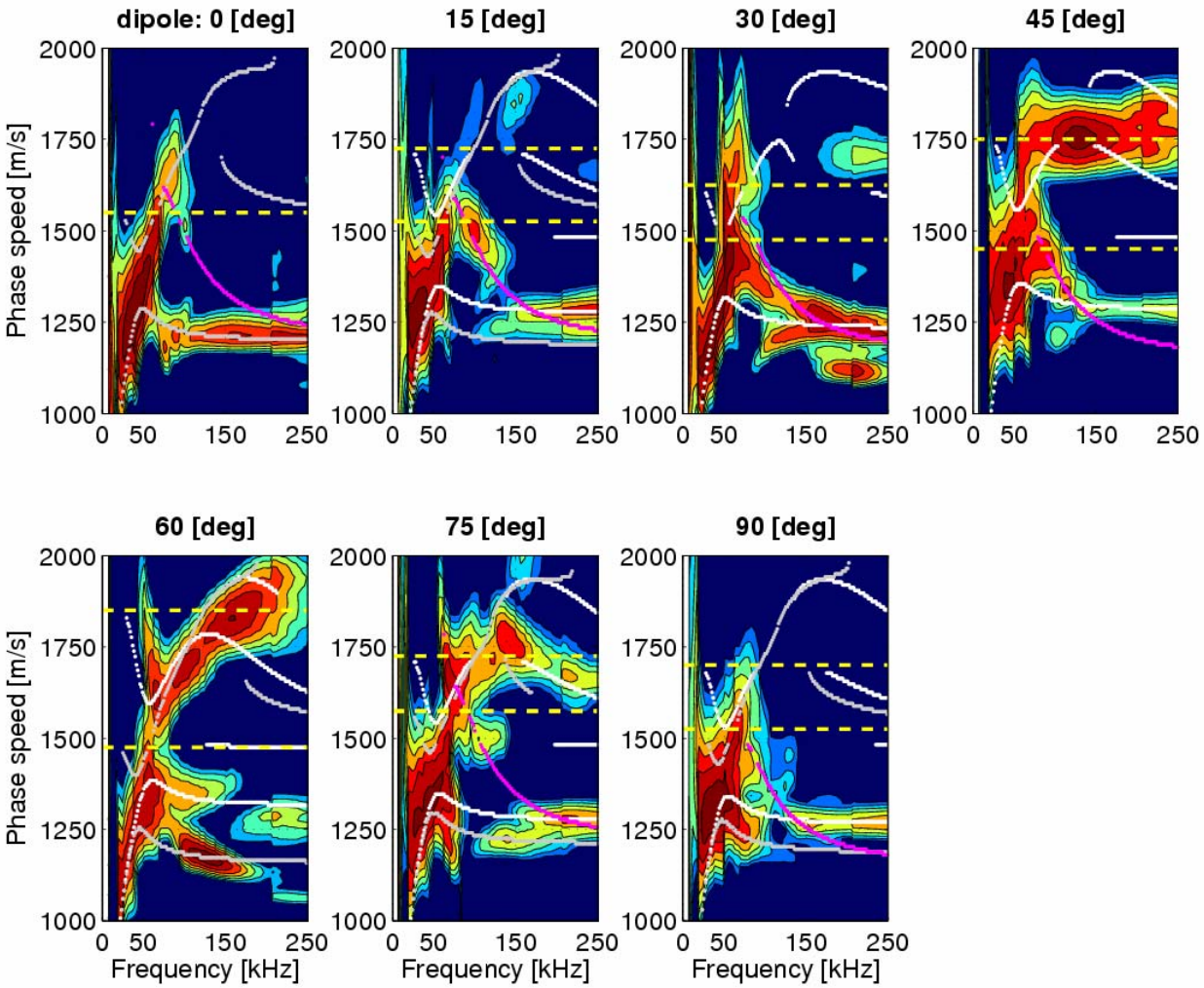

Figure 14: Dipole data at all azimuths – Filtered frequency semblance results with fast dipole (white), slow dipole (gray) and slow hexapole (magenta) modes overlaid, corresponding to a fast and slow formation shear speed (dashed yellow)

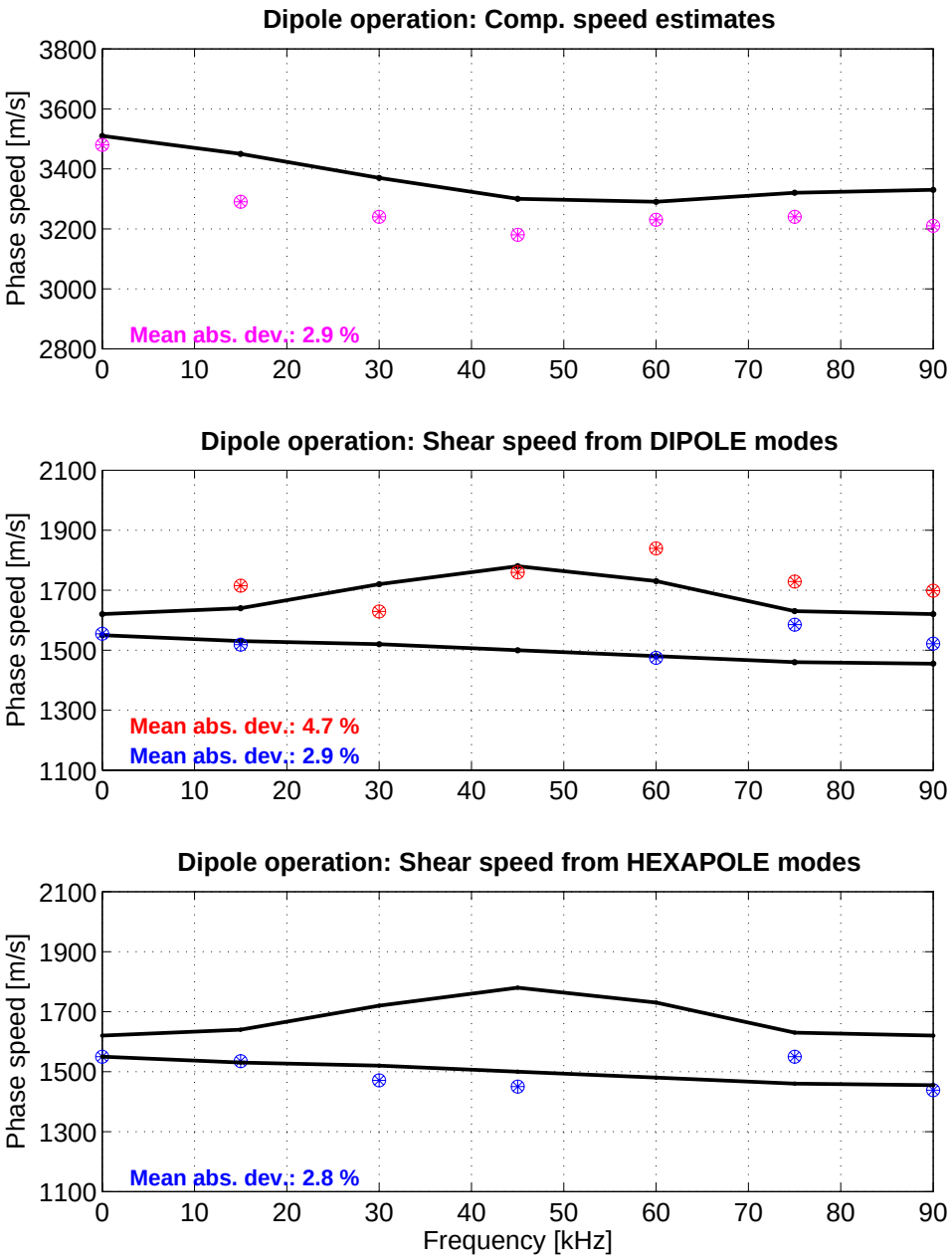

Figure 15 : Dipole operation: Phenolite compression and shear speeds as a function of azimuth, as estimated from scaled LWD measurements. Time of flight measurements are shown as black lines with black markers and LWD measurements are shown as colored markers. Note that the hexapole modes are consistently sensitive only to the slow shear speed

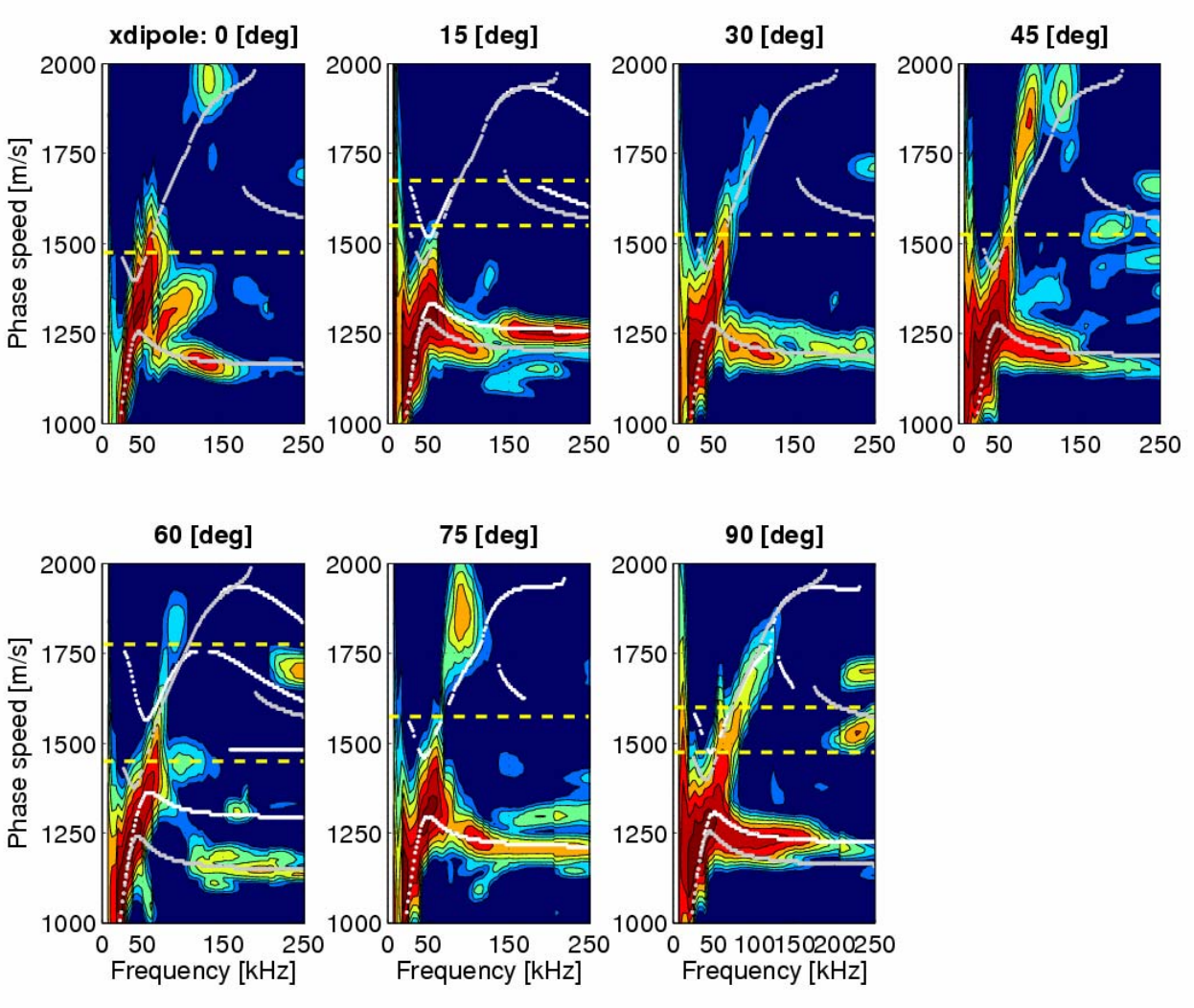

Figure 16 : Cross dipole data at all azimuths – Filtered frequency semblance results with fast dipole (white) and slow dipole (gray) modes overlaid, corresponding to a fast and slow formation shear speed (dashed yellow)

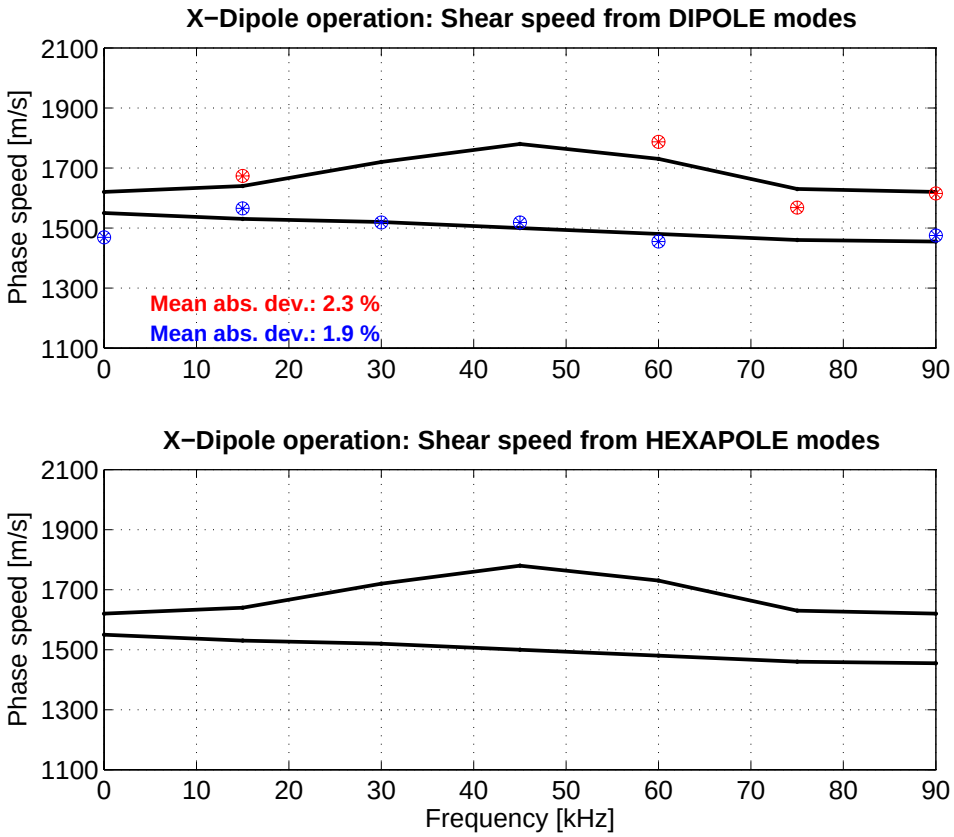

Figure 17 : Cross dipole operation: Phenolite compression and shear speeds as a function of azimuth. Time of flight measurements are shown as black lines with black markers and LWD measurements are shown as colored markers. Note the absence of a hexapole response

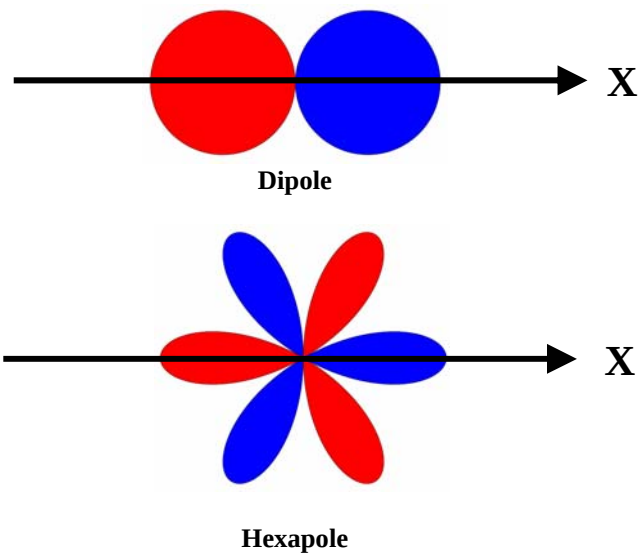

Figure 18: A dipole aligned along X direction has a null along the Y dir (90 and 270 [deg]). A hexapole aligned similarly, has nulls along 30, 90, 150, 210, 270 and 330 [deg]

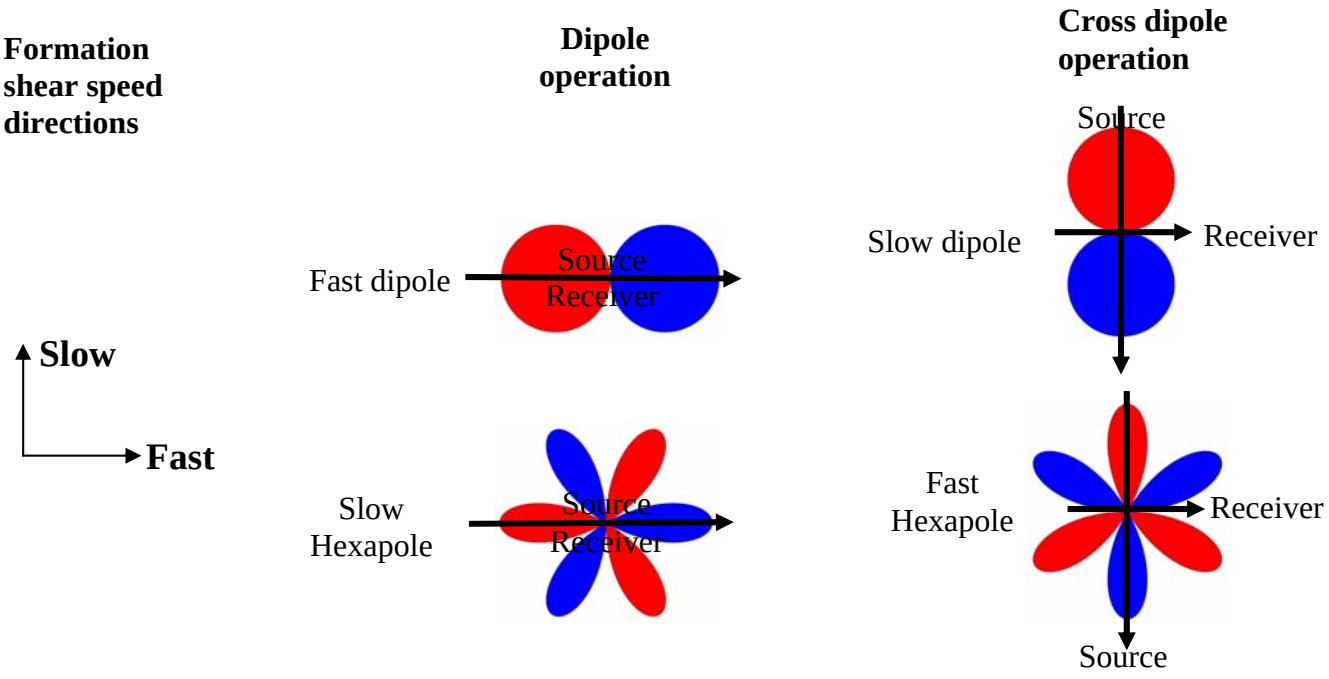

Figure 19: Dipole and Hexapole mode distributions relative to the source/receiver and formation anisotropy orientations for the Dipole and Cross dipole operations